

# Probing the Prompt KV Cache: Where It Becomes Dispensable

Vinayshkhar Bannihatti Kumar   Manoj Ghuhan Arivazhagan\*   Disha Makhija\*  
Rashmi Gangadharaiah

AWS AI Labs

{vinayshk, mghuhan, dismakhi, rgangad}@amazon.com

## Abstract

Prior KV cache compression schemes empirically demonstrate that the prompt cache is partially redundant during decoding, dropping or summarising entries with little accuracy loss. We ask *when* and *what kind* of redundancy. At which layers, after how many decoding steps, and in what form can the prompt span KV cache be replaced without breaking the task. A controlled splice intervention swept over layer cutoff and decoding steps shows this redundancy is about *form* (chat template scaffolding) rather than content. Replacing the upper layer prompt span KV cache with KV cache from a chat template scaffold whose user content is a neutral filler recovers near clean accuracy, while zeroing the same slots collapses accuracy. The dissociation replicates across the Qwen3, Gemma 3, and Llama 3 families on multiple datasets.

## 1 Introduction

A growing body of work hints that LLMs use the prompt differently at different stages of the forward pass. Attention concentrates on the first few positions as a positional sink (Xiao et al., 2024), the same massive activations explain mid-layer compression valleys (Queipo-de Llano et al., 2025), in-context demonstrations are summarised into compact internal task and function vectors (Hendel et al., 2023; Todd et al., 2024), and cross-prompt KV substitution attacks show that generation can be hijacked by overwriting the trailing token positions across all layers of the cache with another prompt’s KV (Ganesh et al., 2025), though that work studies attack feasibility rather than what the cache encodes. KV-cache compression schemes (Cai et al., 2024; Li et al., 2024; Zhang et al., 2023; Ge et al., 2024; Liu et al., 2023) go further and empirically show that large fractions of the prompt cache can be dropped or

summarised with little accuracy loss, indicating partial redundancy. Each line of work, however, addresses the question at a narrow scope (four sink tokens, BOS-token activations, a single task vector, an all-layer-or-nothing swap with one donor pair, or a specific pruning policy) and leaves open the question: When, and with what replacement, can the prompt-span KV cache be replaced: at which layers, after how many decoding steps, and with what donor content? The answer determines whether compression schemes must preserve entries, drop them, or substitute placeholders.

We address this with a controlled splice intervention swept over layer cutoff and decoding steps with donor caches varying in how much of the prompt’s form (chat-template scaffolding) and content (the user’s task) they preserve, tracing a phase diagram of when the prompt-span KV cache can be replaced without breaking the task.

Our contributions are: (i) The first systematic characterisation of *when* the decode-time prompt KV cache becomes dispensable. (ii) *What* of the prompt the cache must retain at upper layers, via a form-vs-content dissociation showing that chat-template scaffolding is sufficient and task content is dispensable, replicated across multiple LLMs and datasets. (iii) A donor-noise ladder over a 180-variant algorithmic-donor benchmark we built to systematically vary noise, in which the donor cache injects increasing amounts of noise (SAME-ALGO → DIFF-ALGO → DIFF-FAMILY). Together these give an end-to-end picture suggesting that at upper layers form alone is sufficient, while at lower layers the cache content is causally consulted, with recovery cost growing as the donor drifts from the target task.

## 2 Models and Datasets

We evaluate Qwen3-4B, Gemma-3-4B-IT, Qwen3-8B, and Llama-3-8B-Instruct (Yang et al.,

\*Equal contribution.

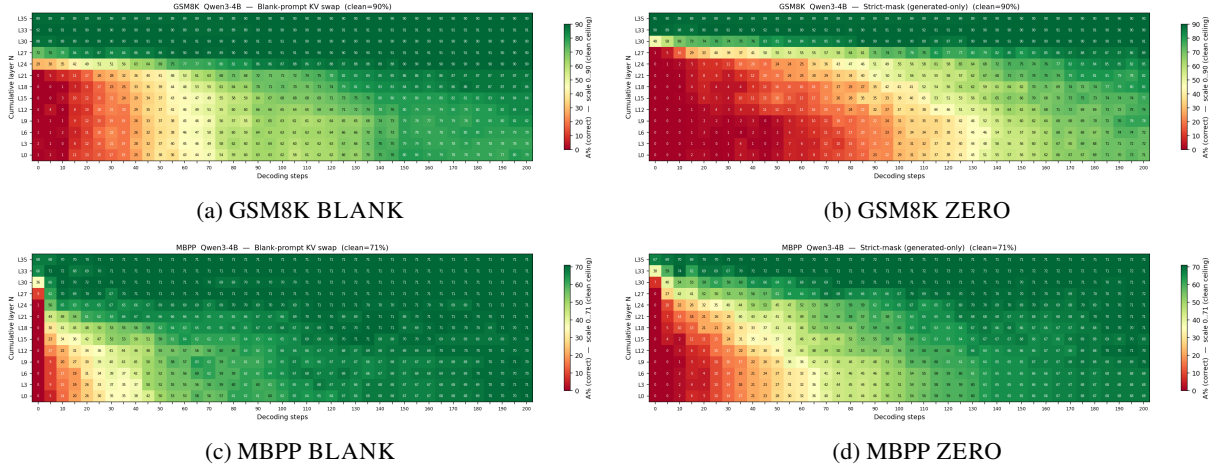


Figure 1: Qwen3-4B heatmaps for ZERO and BLANK on GSM8K (top) and MBPP (bottom). Each cell shows pass% at one  $(L, W)$ . BLANK recovers far faster than ZERO along both  $L$  and  $W$ .

2025; Gemma Team, 2025; Grattafiori et al., 2024), with greedy decoding on four datasets. **GSM8K** (Cobbe et al., 2021) is a standard chain-of-thought arithmetic benchmark, and we score answers by exact match on the final numeric value. **MBPP** (Austin et al., 2021) is a standalone Python code-completion benchmark, and we score completions by passing the test suite shipped with each problem. **HumanEval** (Chen et al., 2021) is a Python function-completion benchmark of 164 hand-written programming problems, each with a function signature, docstring, and hidden unit tests, and we score completions by test-suite pass. From each of the datasets, we sample 100 problems to keep the experiments manageable.

**Algorithmic-donor benchmark.** A Python benchmark spanning 9 algorithmic families (search, sort, graph traversal, shortest path, fibonacci, max-subarray, primes, two-sum, string-match) with 10 LLM-generated problems per family. Each problem appears in two prompt variants that pose the same underlying problem but pin the solution to a different algorithm class (e.g., the same search-family problem is asked once as linear-search and once as binary-search), giving 180 variants indexed by a (problem  $p$ , algorithm-class  $c$ , family  $f$ ) triple, each shipped with a hidden test suite. Correctness is scored as target-algorithm match (via LLM judge) plus test-suite pass.

### 3 Experimental Setup

**Splice intervention.** We study chat-tuned decoder transformers with  $N$  layers. Prefill-

ing on a prompt of length  $T_p$  yields a KV cache  $K^{(\ell)}, V^{(\ell)} \in \mathbb{R}^{T_p \times d}$  at each layer  $\ell \in \{0, \dots, N-1\}$ , and during decoding step  $t$  the model attends over the concatenation of these prompt-span entries with the generated-span entries produced by the previous  $t$  steps.

Every experiment in this paper is an instance of a single intervention parameterised by three quantities, a cumulative layer cutoff  $L$ , a splice onset  $W$  (the number of decoding steps performed before the intervention), and a donor cache  $\tilde{K}, \tilde{V}$ . The cutoff  $L$  defines the patched layer set  $\mathcal{P} = \{\ell : \ell \geq L\}$ , and layers outside  $\mathcal{P}$  are unmodified. The onset  $W$  defines the intervention timing. For decoding steps  $t < W$  the unmodified cache is used, and at step  $t = W$  the prompt-span entries at every layer  $\ell \in \mathcal{P}$  are replaced in place,  $K_{0:T_p}^{(\ell)} \leftarrow \tilde{K}_{0:T_p}^{(\ell)}$  and likewise for  $V$ , after which decoding continues from the modified cache through to completion. Generated-span entries are never modified. The donor cache  $\tilde{K}, \tilde{V}$  takes one of five forms (Table 1). For the three forms produced from an alternate prompt, we trim the longer prompt’s scaffold at the character level until target and donor prompts tokenise to the same length, so the patched slots are positionally aligned.

**Sweep and reporting.** For every (model, task, intervention) we run the full grid  $L \in \{0, 3, 6, \dots, N-1\}$ ,  $W \in \{0, 5, 10, \dots, 200\}$  plus the unintervened *clean* baseline. We summarise each condition as (i) an  $L \times W$  phase-diagram heatmap and (ii) a *recovery frontier*  $W^*(L; \alpha) = \min\{W : \text{pass}(L, W) \geq \alpha p_{\text{clean}}\}$ ,

donor	cache content
ZERO	all-zero $K, V$ at every patched layer
BLANK	chat-template scaffolding with user content replaced by filler token “a” to length $T_p$
SAME-ALGO	donor variant $(p', c, f)$
DIFF-ALGO	donor variant $(p', \neg c, f)$
DIFF-FAMILY	donor variant $(\cdot, \cdot, f')$

Table 1: Donor caches. All interventions modify the same prompt-span positions at the same layers under the same splice onset; only the content varies. Algorithmic-donor variants are indexed by a triple  $(p, c, f)$  of problem  $p$ , algorithm-class  $c$ , family  $f$ .

where  $p_{\text{clean}}$  is the unintervened pass rate of the same model on the same task and  $\alpha \in (0, 1]$ .

## 4 Results and Analysis

### (R1) Form is sufficient, content is dispensable.

We probe whether the prompt cache content matters at upper layers in two steps. We first ask whether *task content* is required at all by running the BLANK intervention (Table 1). Recovery is rapid on both axes (Fig. 1). On Qwen3-4B GSM8K (clean = 90%, median length = 147), BLANK reaches 88% at  $L=30, W=0$ ; sweeping along  $W$  at fixed  $L=27$ , it hits 87% by  $W=25$ . MBPP (clean = 71%, median length = 79) and HumanEval (clean = 79%, median length = 121) reproduces the shape observed in GSM8K. This shows that retaining the prompt’s structural form, while discarding its task content, is sufficient at upper layers.

If task content is not required, what is? We push further and remove the structural scaffolding too via ZERO. Recovery still happens, but is markedly slower on both axes than BLANK. At Qwen3-4B GSM8K  $W = 0$ , ZERO sits at 1% at  $L=27$ , climbs to 48% at  $L=30$ , and only matches clean at  $L=33$ ; along  $W$  at  $L=27$ , it crosses 87% only near  $W \approx 170$ , seven times the pre-splice decoding steps compared to BLANK. MBPP and HumanEval both show the same gap. The two interventions converge at the boundaries. As seen in Fig. 1 both match clean at  $L=33$  and both collapse at shallow  $L$  with  $W=0$ , where no substituted cache can compensate for missing prompt context the model has not yet seen. Hence we can conclude that at upper layers the prompt’s *form* including chat-template scaffolding and positional structure is what must be preserved, while the task *content* carried within can be replaced with a neu-

tral filler.

### (R2) Phase diagram across models and tasks.

The (R1) shape generalises beyond a single model and task. The recovery frontier  $W^*(L; \alpha = 0.75)$  in Fig. 2 plots ZERO (blue) and BLANK (orange) for all four models on GSM8K (top) and MBPP (bottom). On both tasks, BLANK recovers performance faster as BLANK sits consistently to the left of ZERO across every panel of the figure. At intermediate  $L$  the gap is large, on Qwen3-4B GSM8K,  $\sim 60$  steps at  $L = 15$  widening to  $\sim 115$  steps at  $L = 24$ , and both lines collapse to  $W = 0$  only at the topmost cutoffs (BLANK from  $L \approx N-6$  onwards, ZERO a few layers deeper). The gap shrinks for the larger Qwen3-8B but does not invert, and the qualitative pattern of BLANK-to-the-left holds in every panel we plot. We find that the same dissociation holds on the algorithmic-donor benchmark where the BLANK intervention recovers faster than any other donor types (Fig. 3).

### (R3) Donor noise determines lower-layer recovery cost.

At lower layers the prompt cache is no longer dispensable: what gets injected matters, and how much it matters tracks how far the donor cache is from the target. Fig. 3 plots the recovery frontier  $W^*(L; \alpha)$  on the algorithmic-donor benchmark for Qwen3-8B and Llama-3-8B-Instruct at two thresholds ( $\alpha = 0.4, 0.67$ ). BLANK, which preserves only the prompt’s structural form is closest to the  $W=0$  axis at every  $L$ , consistent with (R1): when no task content is injected, decoding recovers fastest. The donor curves degrade as the donor’s content drifts from the target task. The within-family donors (SAME-ALGO and DIFF-ALGO) track each other and require modest pre-splice decoding to recover even at shallow  $L$ ; the across-family donor (DIFF-FAMILY) sits consistently above them, requiring substantially more  $W$  to clear the same threshold. The pattern holds for both Qwen3-8B and Llama-3-8B-Instruct and is sharper at the stricter  $\alpha = 0.67$ , where the gap between DIFF-FAMILY and the within-family lines widens to tens of decoding steps. Together with (R1), these results give an end-to-end picture: at upper layers the model needs only the prompt’s structural form, while at lower layers it actively processes the cache content, with quality degrading as the injected content moves further from the target task. See the appendix for per-model A and per-donor heatmaps F, results on HumanEval dataset E,

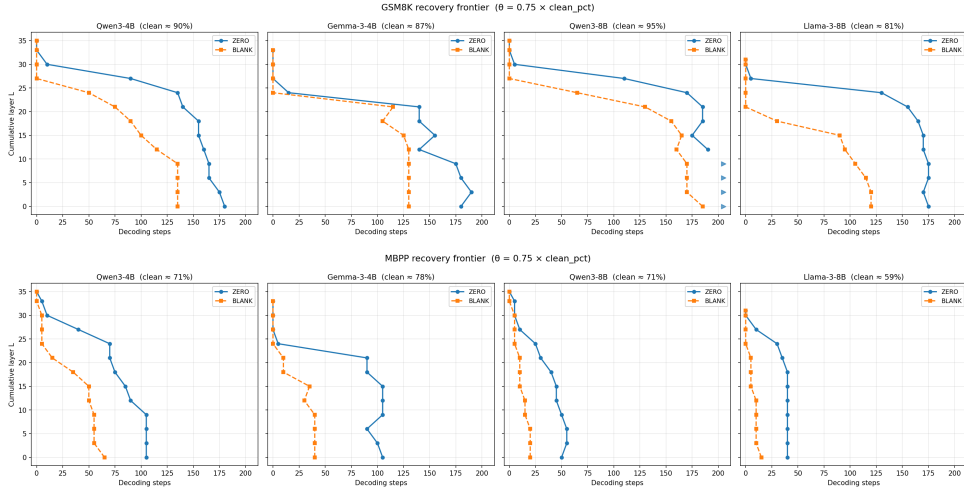


Figure 2: Recovery frontier  $W^*(L; \alpha = 0.75)$  for ZERO (blue) vs BLANK (orange) on GSM8K (top) and MBPP (bottom); columns are the four models. BLANK requires less pre-splice decoding than ZERO at every  $L$ .

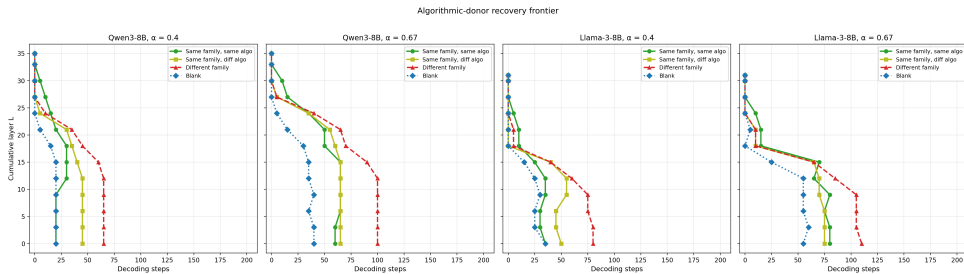


Figure 3: Recovery frontier  $W^*(L; \alpha)$  on the algorithmic-donor benchmark for Qwen3-8B and Llama-3-8B-Instruct at  $\alpha \in \{0.4, 0.67\}$ . Recovery cost grows with donor noise: DIFF-FAMILY (red) is highest, BLANK (blue) lowest.

splice pseudocode C, and example generations D.

## 5 Related Work

Prior work documents prompt-cache redundancy at narrow scopes, including positional sinks at the first  $\sim 4$  tokens (Xiao et al., 2024), mid-layer compression valleys driven by massive activations (Queipo-de Llano et al., 2025), the lost-in-the-middle effect in which models underperform on relevant content placed in the middle of long contexts (Liu et al., 2024), and ICL summarisation into compact internal task and function vectors (Hendel et al., 2023; Todd et al., 2024). A complementary mechanistic line argues that in-context copying is implemented by induction heads, a distributed attention pattern rather than a vector summary (Olsson et al., 2022). KV-cache compression schemes (Cai et al., 2024; Li et al., 2024; Zhang et al., 2023; Ge et al., 2024; Liu et al., 2023) prune by attention magnitude, and our results suggest a complementary axis of substitution by structural placeholders at upper layers.

Ganesh et al. (2025) is the closest methodologically, an attack feasibility study that hijacks generation by overwriting trailing token positions across all KV layers with fixed donor. We ask a different question and run a graded donor-noise ladder, expose an algorithmic-overlap inversion, and add the form-vs-content ZERO-vs-BLANK dissociation.

## 6 Conclusion

A controlled splice intervention across layers and decoding steps reveals a depth-dependent split in what the prompt KV cache must carry. At upper layers, chat-template alone is sufficient: content-free filler recovers near-clean accuracy while zeroing the same slots collapses generation. At lower layers, content is causally active: donor caches degrade accuracy in proportion to their distance from the target task, with cross-family donors requiring substantially more decoding steps to recover than within-family donors. For KV-cache compression, the practical implication is that upper-layer prompt entries can be replaced with structural placeholder-

ers rather than dropped, while lower-layer entries must preserve task-specific content.

## Limitations

Our splice intervention requires write access to the prompt-span key/value cache, which restricts the analysis to settings where model internals can be modified at inference time. It does not directly characterise behaviour observable through standard inference APIs. The study covers four chat-tuned decoder-only transformers in the 4B to 8B parameter range and three task domains alongside an algorithmic-donor benchmark. We have not investigated encoder-decoder architectures, base models without instruction tuning, or substantially larger models. The absolute layer depth at which form alone becomes sufficient is reported per model rather than predicted from architectural quantities. Finally, our BLANK construction relies on a chat-template scaffold filled with a single neutral filler token. This isolates form from content cleanly but does not distinguish which structural elements such as role markers, length, position, or specific template tokens carry the load. We leave a finer decomposition of form to future work.

## References

- Jacob Austin, Augustus Odena, Maxwell Nye, Maarten Bosma, Henryk Michalewski, David Dohan, Ellen Jiang, Carrie Cai, Michael Terry, Quoc Le, and Charles Sutton. 2021. Program synthesis with large language models. *arXiv preprint arXiv:2108.07732*.
- Zefan Cai, Yichi Zhang, Bofei Gao, Yuliang Liu, Yucheng Li, Tianyu Liu, Keming Lu, Wayne Xiong, Yue Dong, Junjie Hu, and Wen Xiao. 2024. PyramidKV: Dynamic KV cache compression based on pyramidal information funneling. *arXiv preprint arXiv:2406.02069*.
- Mark Chen, Jerry Tworek, Heewoo Jun, Qiming Yuan, Henrique Ponde de Oliveira Pinto, Jared Kaplan, Harri Edwards, Yuri Burda, Nicholas Joseph, Greg Brockman, and 1 others. 2021. Evaluating large language models trained on code. *arXiv preprint arXiv:2107.03374*.
- Karl Cobbe, Vineet Kosaraju, Mohammad Bavarian, Mark Chen, Heewoo Jun, Lukasz Kaiser, Matthias Plappert, Jerry Tworek, Jacob Hilton, Reiichiro Nakano, Christopher Hesse, and John Schulman. 2021. Training verifiers to solve math word problems. *arXiv preprint arXiv:2110.14168*.
- Mukesh Ganesh, Kaushik Iyer, and Arun Baalaji Sankar Ananthan. 2025. Whose narrative is it anyway? a KV cache manipulation attack. *arXiv preprint arXiv:2511.12752*.
- Suyu Ge, Yunan Zhang, Liyuan Liu, Minjia Zhang, Jiawei Han, and Jianfeng Gao. 2024. Model tells you what to discard: Adaptive KV cache compression for LLMs. In *International Conference on Learning Representations (ICLR)*.
- Gemma Team. 2025. Gemma 3 technical report. *arXiv preprint arXiv:2503.19786*.
- Aaron Grattafiori, Abhimanyu Dubey, Abhinav Jauhri, Abhinav Pandey, Abhishek Kadian, Ahmad Al-Dahle, Aiesha Letman, Akhil Mathur, Alan Schelten, Alex Vaughan, and 1 others. 2024. The Llama 3 herd of models. *arXiv preprint arXiv:2407.21783*.
- Roe Hendel, Mor Geva, and Amir Globerson. 2023. In-context learning creates task vectors. In *Findings of the Association for Computational Linguistics: EMNLP 2023*.
- Yuhong Li, Yingbing Huang, Bowen Yang, Bharat Venkitesh, Acyr Locatelli, Hanchen Ye, Tianle Cai, Patrick Lewis, and Deming Chen. 2024. SnapKV: LLM knows what you are looking for before generation. *arXiv preprint arXiv:2404.14469*.
- Nelson F. Liu, Kevin Lin, John Hewitt, Ashwin Paranjape, Michele Bevilacqua, Fabio Petroni, and Percy Liang. 2024. Lost in the middle: How language models use long contexts. *Transactions of the Association for Computational Linguistics*, 12:157–173.
- Zichang Liu, Aditya Desai, Fangshuo Liao, Weitao Wang, Victor Xie, Zhaozhuo Xu, Anastasios Kyrillidis, and Anshumali Shrivastava. 2023. Scissorhands: Exploiting the persistence of importance hypothesis for LLM KV cache compression at test time. In *Advances in Neural Information Processing Systems (NeurIPS)*.
- Catherine Olsson, Nelson Elhage, Neel Nanda, Nicholas Joseph, Nova DasSarma, Tom Henighan, Ben Mann, Amanda Askell, Yuntao Bai, Anna Chen, Tom Conerly, Dawn Drain, Deep Ganguli, Zac Hatfield-Dodds, Danny Hernandez, Scott Johnston, Andy Jones, Jackson Kernion, Liane Lovitt, and 7 others. 2022. In-context learning and induction heads. Transformer Circuits Thread.
- Enrique Queipo-de Llano, Álvaro Arroyo, Federico Barbero, Xiaowen Dong, Michael Bronstein, Yann LeCun, and Ravid Shwartz-Ziv. 2025. Attention sinks and compression valleys in LLMs are two sides of the same coin. *arXiv preprint arXiv:2510.06477*.
- Eric Todd, Millicent L. Li, Arnab Sen Sharma, Aaron Mueller, Byron C. Wallace, and David Bau. 2024. Function vectors in large language models. In *International Conference on Learning Representations (ICLR)*.

Guangxuan Xiao, Yuandong Tian, Beidi Chen, Song Han, and Mike Lewis. 2024. [Efficient streaming language models with attention sinks](#). In *International Conference on Learning Representations (ICLR)*.

An Yang, Anfeng Li, Baosong Yang, Beichen Zhang, Binyuan Hui, Bo Zheng, Bowen Yu, Chang Gao, Chengen Huang, Chenxu Lv, Chujie Zheng, Dayiheng Liu, Fan Zhou, Fei Huang, Feng Hu, Hao Ge, Haoran Wei, Huan Lin, Jialong Tang, and 41 others. 2025. Qwen3 technical report. *arXiv preprint arXiv:2505.09388*.

Zhenyu Zhang, Ying Sheng, Tianyi Zhou, Tianlong Chen, Lianmin Zheng, Ruisi Cai, Zhao Song, Yuandong Tian, Christopher Ré, Clark Barrett, Zhangyang Wang, and Beidi Chen. 2023. [H<sub>2</sub>O: Heavy-hitter oracle for efficient generative inference of large language models](#). In *Advances in Neural Information Processing Systems (NeurIPS)*.

## Appendix

### A Per-Model Phase Diagrams

Fig. 1 in the main text shows phase diagrams for Qwen3-4B only. Fig. 4 provides the analogous per-cell heatmaps for Gemma-3-4B-IT, Qwen3-8B, and Llama-3-8B-Instruct on both GSM8K and MBPP, for both ZERO and BLANK. Across every (model, task) pair, the same pattern holds. BLANK cells stay near the clean baseline once  $L$  is sufficiently deep, while ZERO cells form a red region at shallow  $L$  that contracts only at the topmost cut-offs.

### B Clean Baselines

Table 2 reports the unintervened (*clean*) pass rate  $p_{\text{clean}}$  used as the reference in the recovery frontier  $W^*(L; \alpha) = \min\{W : \text{pass}(L, W) \geq \alpha p_{\text{clean}}\}$ . Each entry is the pass rate of the unmodified model on the full benchmark sample (100 items for GSM8K, 100 items for MBPP), computed once per (model, task) pair and shared across all interventions.

model	GSM8K	MBPP	HumanEval
Qwen3-4B	90.0	71.0	79.0
Gemma-3-4B-IT	87.0	78.0	71.0
Qwen3-8B	95.0	71.0	77.0
Llama-3-8B-Instruct	81.0	59.0	59.0

Table 2: Clean baselines  $p_{\text{clean}}$  (% , exact match for GSM8K, test-suite pass for MBPP and HumanEval) for the four models evaluated.

### C Splice Intervention Pseudocode

Algorithm 1 restates the splice intervention as a modified greedy decoding loop. The loop differs from a standard greedy decode only in line 5, which performs a single in-place replacement of the prompt-span entries at the patched layers once decoding has reached step  $W$ . The patched cache is then used for every subsequent decoding step until generation terminates.

### D Example Generations

To complement the aggregate pass-rate results, Tables 3 and 4 report side-by-side greedy completions from Qwen3-4B on representative MBPP and GSM8K problems at ( $L = 27, W = 0$ ), the regime where the ZERO vs BLANK gap is largest while BLANK is still recoverable. Each row shows

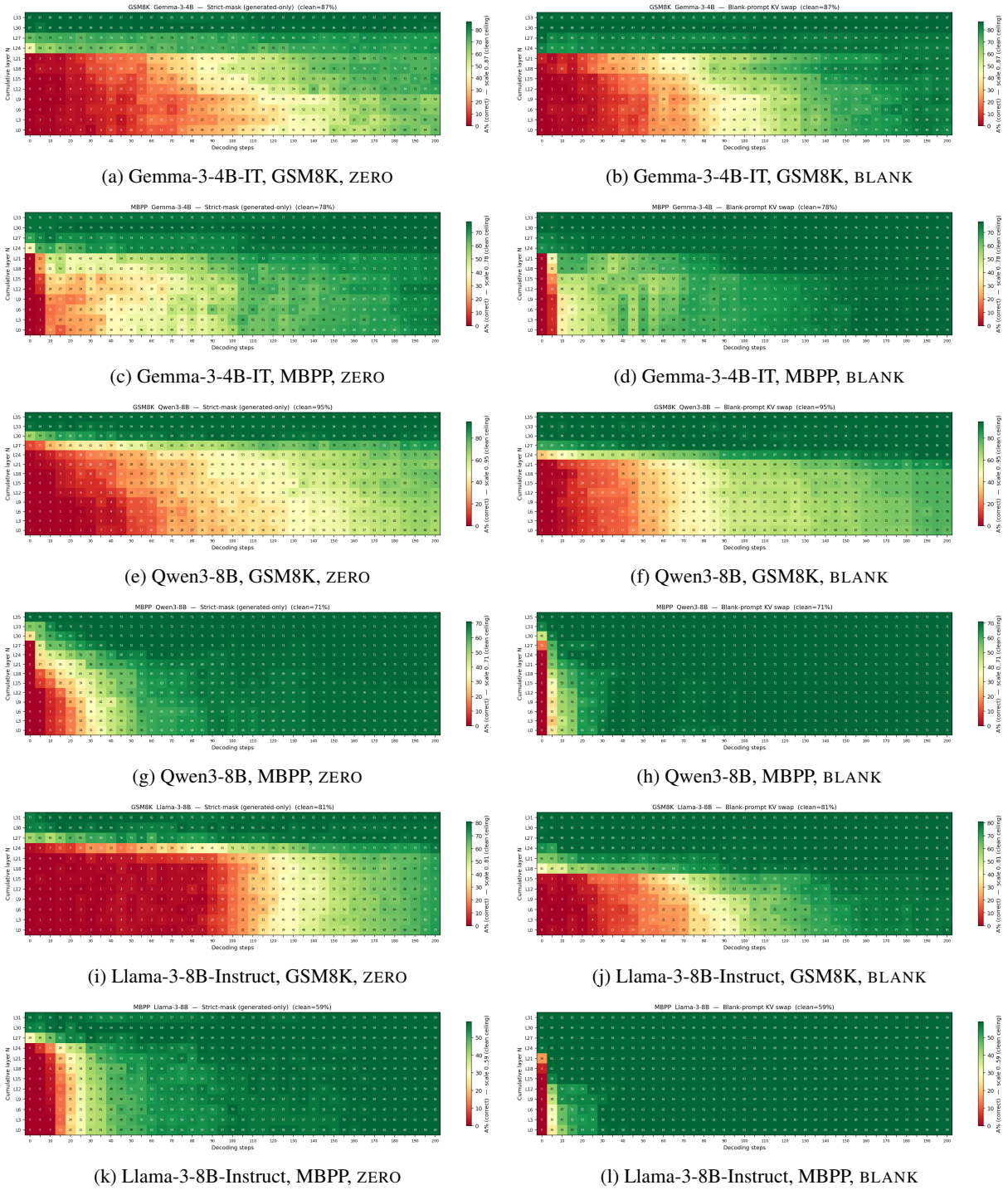


Figure 4: Per-cell heatmaps for Gemma-3-4B-IT, Qwen3-8B, and Llama-3-8B-Instruct on GSM8K and MBPP. Each cell is a pass-rate percentage at one  $(L, W)$  configuration. Rows within a panel are cumulative layer cutoffs, columns are pre-splice decoding steps  $W$ . The left column shows ZERO and the right column shows BLANK. Across every (model, task) pair, BLANK stays near the clean baseline at deep  $L$  while ZERO produces a large red region at shallow  $L$  that only contracts at the topmost cutoffs.

---

**Algorithm 1** Splice-intervention greedy decode

---

**Require:** model  $M$  with  $N$  layers, prefilled cache  $(K, V)$  with prompt-span length  $T_p$ , donor cache  $(\tilde{K}, \tilde{V})$ , layer cutoff  $L$ , splice onset  $W$ , max new tokens  $T_{\max}$

- 1:  $\mathcal{P} \leftarrow \{\ell : \ell \geq L\}$   $\triangleright$  patched layers
- 2:  $y_0 \leftarrow \arg \max_v M_{\text{logits}}(K, V)_v$
- 3:  $tokens \leftarrow [y_0]$
- 4: **for**  $t = 1$  to  $T_{\max} - 1$  **do**
- 5:     **if**  $t = W$  **then**
- 6:         **for**  $\ell \in \mathcal{P}$  **do**
- 7:              $K_{0:T_p}^{(\ell)} \leftarrow \tilde{K}_{0:T_p}^{(\ell)}$
- 8:              $V_{0:T_p}^{(\ell)} \leftarrow \tilde{V}_{0:T_p}^{(\ell)}$
- 9:         **end for**
- 10:     **end if**
- 11:      $(K, V) \leftarrow M(tokens[t-1], (K, V))$   $\triangleright$  forward pass, appends generated KV to cache
- 12:      $y_t \leftarrow \arg \max_v M_{\text{logits}}(K, V)_v$
- 13:     **if**  $y_t = \text{eos}$  **then break**
- 14:     **end if**
- 15:      $tokens.append(y_t)$
- 16: **end for**
- 17: **return**  $tokens$

---

the output under the unintervened decode, the BLANK intervention, and the ZERO intervention. Visible characters are verbatim from the decoded output, problem statements are paraphrased to a single line, and “...” marks elided text. In ZERO cells this is further token-loop repetition, and in CLEAN or BLANK cells this is surrounding prose.

## E HumanEval Replication

The form-vs-content dissociation also replicates on HumanEval (Chen et al., 2021). Fig. 5 shows the recovery frontier  $W^*(L; \alpha = 0.75)$  for ZERO and BLANK on all four models, and Fig. 6 gives the per-cell phase diagrams. Across every model, BLANK sits to the left of ZERO and reaches near-baseline at deep  $L$  while ZERO requires substantially more pre-splice decoding to recover.

## F Per-Model Heatmaps on the Algorithmic-Donor Benchmark

Fig. 7 gives a unified cell-level view of the algorithmic-donor benchmark across the four models and four donor caches, under both test-pass scoring and an algo-aware score that additionally checks whether the emitted solution uses the prescribed algorithm class. Reading

across columns reproduces the noise ladder of (R3). Damage grows from BLANK and SAME-ALGO through DIFF-ALGO to DIFF-FAMILY. The two scoring rules diverge most under DIFF-ALGO, where the model passes the tests but commits to the donor’s algorithm class, so the algo-aware column develops a large red region that persists to deeper  $L$ .

## G Algorithmic-Donor Benchmark Construction

The algorithmic-donor benchmark is built around a hand-written taxonomy of algorithm pairs. Each pair shares an input/output contract but admits two distinct algorithmic strategies, an A side (typically a naive baseline) and a B side (typically an optimised alternative). Nine pairs were specified in this taxonomy. The pairs cover search (linear vs binary), sort (bubble vs merge), graph traversal (BFS vs DFS), shortest path (Dijkstra vs Bellman-Ford), Fibonacci (naive recursion vs bottom-up DP), max-subarray (brute force vs Kadane), primes (trial division vs Sieve of Eratosthenes), two-sum (nested-loop vs hash-map single pass), and string match (naive vs KMP). Each taxonomy entry is paired with a short natural-language description of the contract and the strategy.

**Variant generation:** Sonnet 4.5 (max\_tokens=4096, temperature=0.8) was used in the dataset construction. The system prompt used in this pass is show below.

### Variant Generation System Prompt

```
You are a programming problem generator. Given an algorithm family with algorithms A and B, generate exactly 10 diverse problem variants. Each variant should be a different concrete problem (different domain, data types, or scenario) that both algorithms can solve.
```

```
For each variant, provide:  
1. A Python prompt asking for algorithm B  
2. A Python solution using algorithm A
```

```
Return a JSON array of 10 objects, each with keys:  
- 'variant_name': short description  
- 'python_b_prompt': one-sentence Python prompt explicitly naming algorithm B
```

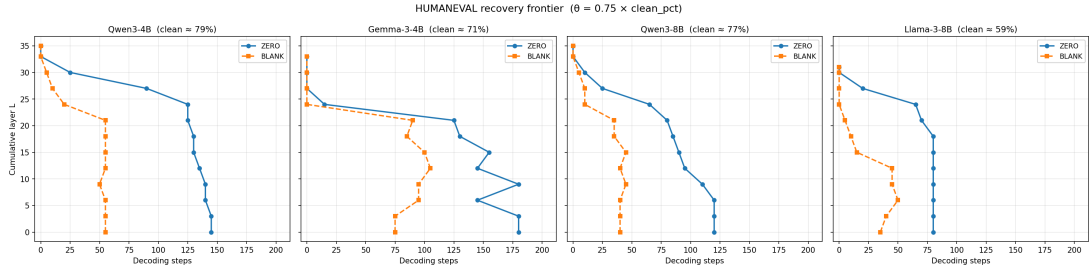


Figure 5: HumanEval recovery frontier  $W^*(L; \alpha = 0.75)$  for ZERO (blue) and BLANK (orange), one panel per model. BLANK sits consistently to the left of ZERO across every model.

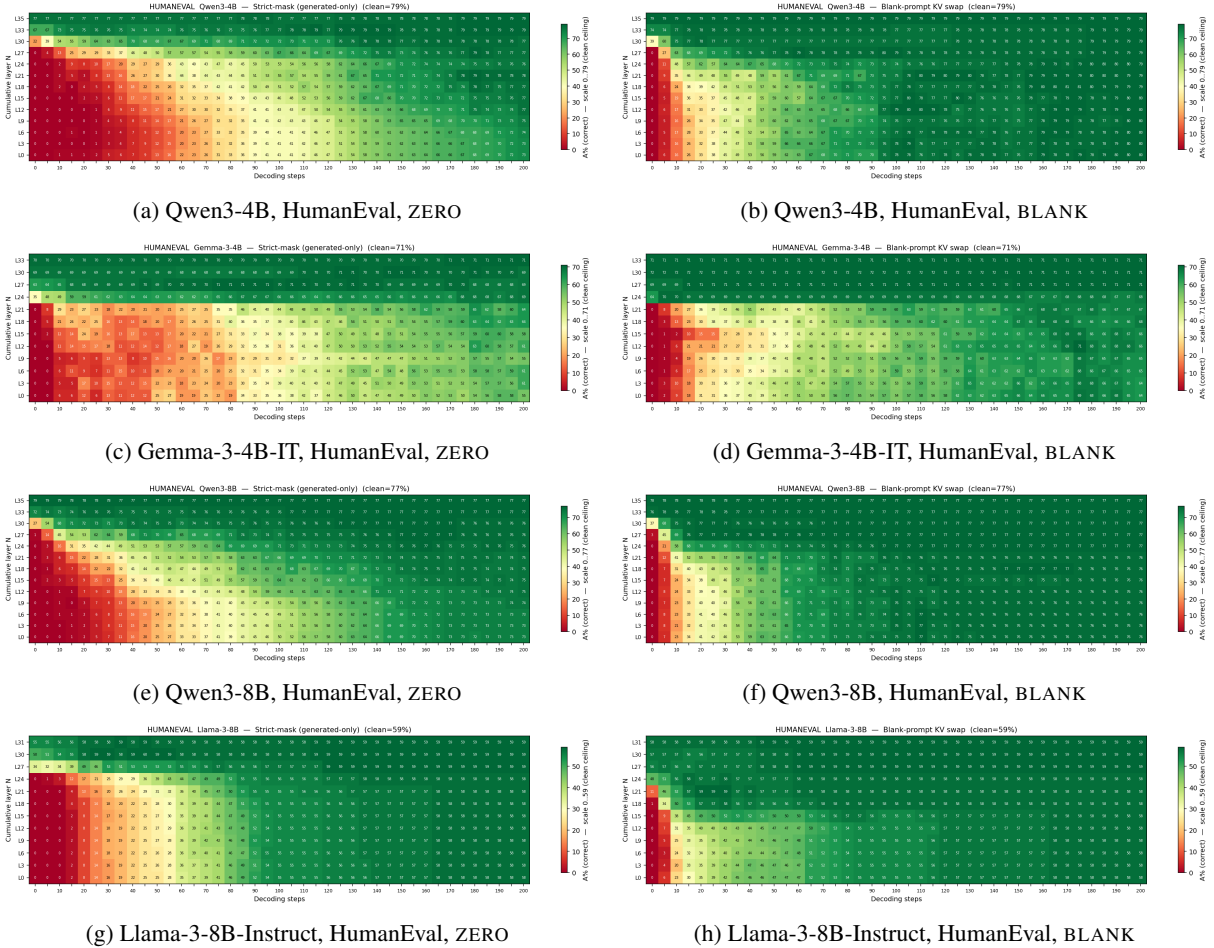


Figure 6: Per-cell heatmaps on HumanEval for the four models, one row per model. The left column shows ZERO and the right column shows BLANK. Each cell is a pass-rate percentage at one  $(L, W)$  configuration. Rows within a panel are cumulative layer cutoffs, columns are pre-splice decoding steps  $W$ . BLANK stays near the clean baseline at deep  $L$ , while ZERO produces a large red region at shallow  $L$  that only contracts at the topmost cutoffs.

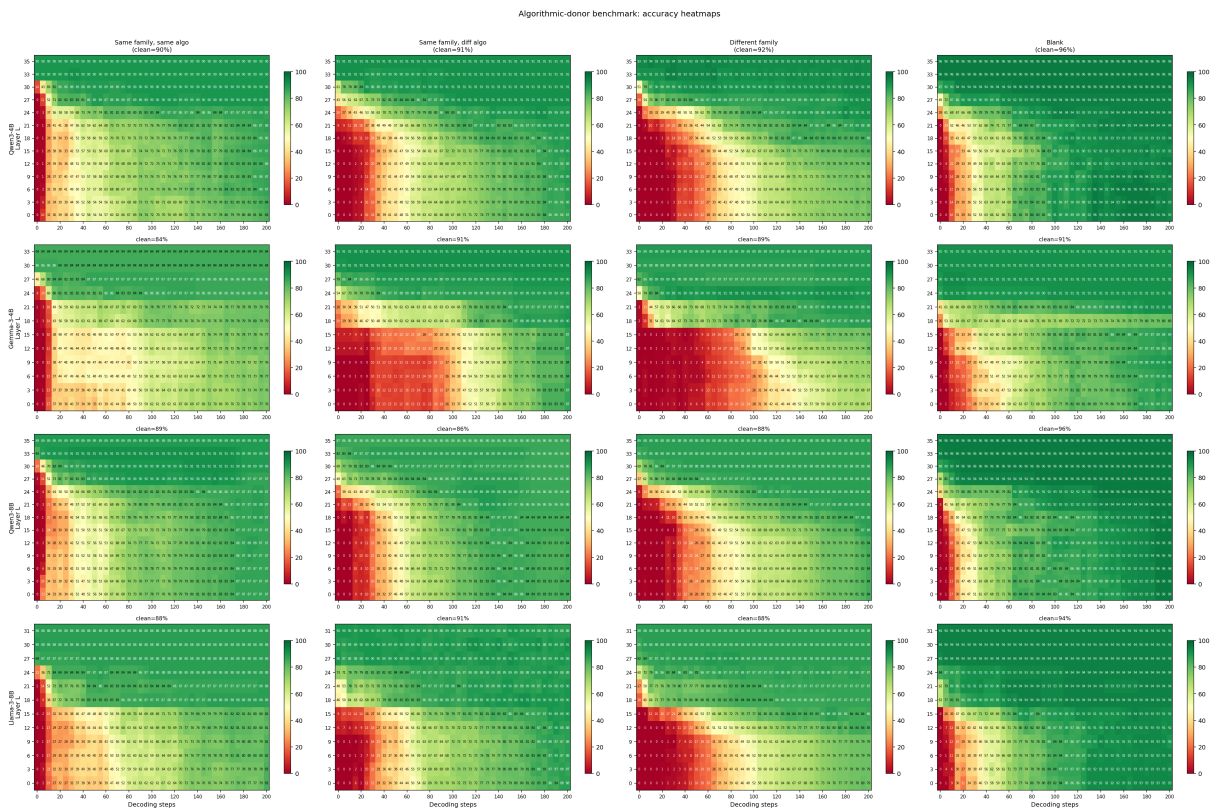


Figure 7: Unified per-cell heatmaps on the algorithmic-donor benchmark. Rows are models (Qwen3-4B, Gemma-3-4B-IT, Qwen3-8B, Llama-3-8B-Instruct), and columns group the four donor caches (BLANK, SAME-ALGO, DIFF-ALGO, DIFF-FAMILY) under test-pass scoring and an algo-aware score that also requires the emitted solution to use the prescribed algorithm class.

problem	CLEAN	BLANK	ZERO
string_to_list: split a string on whitespace	def string_to_list(s): return s.split()	def string_to_list(s): return s.split()	def armour_arm_arm_arm_arm_arm...
find_star_num: nth centered hexago- nal number	def find_star_num(n): # The formula for the n'th # star number is 6n(n-1) + 1 return 6 * n * (n - 1) + 1	def a(n): return 6 * n * n - 6 * n + 1	def get_get_get_get_get_get...

Table 3: Greedy completions from Qwen3-4B on two MBPP problems under the uninvolved (CLEAN) decode, the BLANK intervention, and the ZERO intervention, all at  $L = 27, W = 0$ . Under BLANK the model emits well-formed, mostly correct Python. For `string_to_list` the completion is identical to the uninvolved output, and for `find_star_num` it produces an equivalent closed form ( $6n^2 - 6n + 1$  vs.  $6n(n-1) + 1$ ) but under a renamed entry point (`a`), which would fail a strict test harness despite the formula being correct. Under ZERO the decoder collapses into a single-token loop and produces no usable solution.

problem	CLEAN	BLANK	ZERO
Dog grooming costs \$100, 30% discount, price after?	...discount amount is \$100 × 0.30 = \$30. Subtracting... \$70. The answer is 70. ✓	...10% of \$100 is \$10. So the discounted price is \$100 - \$10 = \$90. The answer is 90. ✗	The original cost of the dog dog dog dog dog dog dog dog dog dog dog dog... ✗
Lily has 50 friends, Amy has 20 more, to- tal?	...Amy made 50 + 20 = 70 friends. Together 70 + 50 = 120 friends. ✓	...Ava has 20 more friends than Lia... 50 + 20 = 70... (truncated)	We know that and and and and and and and and and and and and... ✗

Table 4: Greedy completions from Qwen3-4B on two GSM8K problems under the uninvolved (CLEAN) decode, the BLANK intervention, and the ZERO intervention, all at  $L = 27, W = 0$ . Reference (gold) answers are 70 and 120. Under CLEAN the model follows a coherent arithmetic chain and reaches the gold answer in both cases. Under BLANK the decoder remains arithmetic and roughly on-topic but introduces small content errors, such as misreading the discount rate in the first problem and renaming the protagonists in the second, resulting in incorrect final answers. Under ZERO the model emits a degenerate single-token loop and never produces a numeric answer.

```
- ``python_a_code``: complete Python
function implementing algorithm A

Return ONLY valid JSON, no prose.
```

The user prompt provided the family name, the names of algorithms A and B, and an example A-side and B-side prompt drawn from the taxonomy. The output was constrained to a JSON array of ten objects per family. Each call was retried up to three times on parse or transport errors with a short sleep between retries.

**Flipped halves.** Using the same model at `temperature=0.2` and the same other settings, the system prompt provided the existing A-side Python implementation and the name of algorithm B and asked for two outputs, a Python implementation of algorithm B with the identical function signature, and a Python prompt requesting algo-

rithm A for the same problem. The user prompt repeated the algorithm names, embedded the existing A-side Python code, and quoted the original B-side Python prompt for context. After this pass each variant carries all four artifacts, an A-side prompt and reference implementation in Python and a B-side prompt and reference implementation in Python.

**Ground truth and tests.** The committed ground-truth file holds, per variant, two prompt sides (A-side and B-side) plus a deterministic test suite of five cases (one edge case and four normal). Reference Python implementations were produced as a generation-pipeline artifact and are checked for internal consistency, but the splice experiments only use the prompts and test cases. Across the nine families with ten variants each, this yields ninety problems and one hundred and eighty prompt variants in total, indexed by a

(problem  $p$ , algorithm-class  $c$ , family  $f$ ) triple.

## **H Example Generations on the Algorithmic-Donor Benchmark**

Tables 5 and 6 show greedy completions from Qwen3-4B under all four donor interventions at ( $L=12, W=15$ ). Each entry illustrates the characteristic failure mode of that donor condition.

condition	generated code (truncated)
BLANK	<p><b>Target:</b> Sort file sizes in descending order using merge sort.</p> <p><b>Output:</b></p> <pre>def sort_file_sizes_descending(sizes):     if len(sizes) == 0:         return []     return sorted(sizes, reverse=True)</pre> <p><b>Result:</b> 5/5 tests pass. Uses built-in <code>sorted()</code> instead of merge sort. The blank cache carries no algorithm-class signal, so the model defaults to the simplest correct implementation.</p>
SAME-ALGO	<p><b>Target:</b> Sort 2D coordinates by distance from origin (merge sort).</p> <p><b>Donor:</b> Sort RGB colors by brightness (merge sort).</p> <p><b>Output:</b></p> <pre>def sort_points_by_distance(points): # target name     def get_brightness(color): # donor logic         return 0.299*color[0] + 0.587*color[1] + ...     def merge_sort(arr): ... # correct algo</pre> <p><b>Result:</b> 1/5 tests, <code>exec.error</code>. Correct algorithm (merge sort) and target function name, but the comparison helper uses the <i>donor's</i> brightness logic instead of Euclidean distance. Hybrid of target signature + donor identifiers <math>\rightarrow</math> <code>NameError</code>.</p>

Table 5: Algorithmic-donor examples (1/2): BLANK and SAME-ALGO at  $L=12$ , decoding step=15, Qwen3-4B.

condition	generated code (truncated)
DIFF-ALGO	<p><b>Target:</b> Sort 2D coordinates by distance from origin (merge sort).</p> <p><b>Donor:</b> Sort email addresses by domain (bubble sort).</p> <p><b>Output:</b></p> <pre>def sort_points_by_distance(points): # target name     def bubble_sort(arr): # donor algo         for i in range(len(arr)):             for j in range(0, len(arr)-i-1):                 domain1 = arr[j].split('@')[1] # donor logic                 domain2 = arr[j+1].split('@')[1]                 ...</pre> <p><b>Result:</b> 1/5 tests, fail. Switches to the donor's algorithm (bubble sort) <i>and</i> the donor's domain logic (email parsing). The entire algorithmic strategy flips to the donor's, not just the identifiers.</p>
DIFF-FAMILY	<p><b>Target:</b> Sort 2D coordinates by distance from origin (merge sort).</p> <p><b>Donor:</b> Prime gap calculation (primes family).</p> <p><b>Output:</b></p> <pre>def sort_points_by_distance(points): # target name     def is_prime(num): # donor family         if num &lt; 2: return False         for i in range(3, int(math.isqrt(num))+1, 2):             if num % i == 0: return False         return True     primes = []     for num in ...</pre> <p><b>Result:</b> 0/5 tests, <code>exec.error</code>. Retains the target's function name but implements a prime sieve (donor's family). The donor cache is so distant that the model cannot recover any aspect of the target task.</p>

Table 6: Algorithmic-donor examples (2/2): DIFF-ALGO and DIFF-FAMILY at  $L=12$ , decoding step=15, Qwen3-4B. Together with Table 5, these illustrate the graded noise ladder: BLANK loses the algorithm class but produces correct output; SAME-ALGO preserves the algorithm but leaks donor identifiers; DIFF-ALGO flips the algorithm entirely; DIFF-FAMILY produces an unrelated computation.